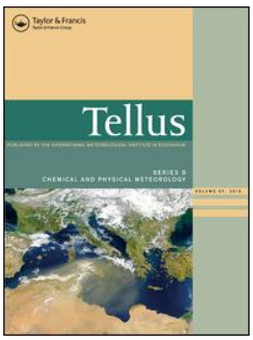

Tellus B: Chemical and Physical Meteorology

ISSN: (Print) 1600-0889 (Online) Journal homepage: http://www.tandfonline.com/loi/zelb20

The observed relationship of cloud to surface longwave radiation and air temperature at Ny-Ålesund, Svalbard

Huidong Yeo, Sang-Jong Park, Baek-Min Kim, Masataka Shiobara, Sang-Woo Kim, Hataek Kwon, Joo-Hong Kim, Jee-Hoon Jeong, Sang Seo Park & Taejin Choi

To cite this article: Huidong Yeo, Sang-Jong Park, Baek-Min Kim, Masataka Shiobara, Sang-Woo Kim, Hataek Kwon, Joo-Hong Kim, Jee-Hoon Jeong, Sang Seo Park & Taejin Choi (2018) The observed relationship of cloud to surface longwave radiation and air temperature at Ny-Ålesund, Svalbard, Tellus B: Chemical and Physical Meteorology, 70:1, 1450589, DOI: 10.1080/16000889.2018.1450589

To link to this article: https://doi.org/10.1080/16000889.2018.1450589

Tellus SERIES B CHEMICAL AND PHYSICAL METEOROLOGY
PUBLISHED BY THE INTERNATIONAL METEOROLOGICAL INSTITUTE IN STOCKHOLM

The observed relationship of cloud to surface longwave radiation and air temperature at Ny-Ålesund, Svalbard

By HUIDONG YEO[1], SANG-JONG PARK[2], BAEK-MIN KIM[2], MASATAKA SHIOBARA[3], SANG-WOO KIM[1*], HATAEK KWON[2], JOO-HONG KIM[2], JEE-HOON JEONG[4], SANG SEO PARK[1] and TAEJIN CHOI[2], [1]*School of Earth and Environmental Sciences, Seoul National University, Seoul, Korea;* [2]*Korea Polar Research Institute, Incheon, Korea;* [3]*National Institute of Polar Research, Tokyo, Japan;* [4]*Department of Oceanography, Chonnam National University, Gwangju, Korea*

(Manuscript received 6 April 2017; in final form 5 March 2018)

ABSTRACT

Ten-year (2004–2013) observations of cloud and surface shortwave (SW) and longwave (LW) fluxes at Ny-Ålesund were analysed to investigate monthly variations in cloudiness and their impacts on the surface LW radiation budget and near-surface temperature (T_s). The cloud fraction (CF) showed distinct monthly variations, high in summer (0.90) and lower in winter (0.79). The downward SW flux increased from March and showed a peak (~200 W m^{-2}) in June. In contrast, the downward LW (LWD) flux increased from ~200 W m^{-2} in February to ~300 W m^{-2} in July. Both LWD and upward LW (LWU) fluxes and their difference increased during winter as lowest cloud base height (LCBH) decreased and CF increased. T_s difference and both LW fluxes difference (ΔLWD and ΔLWU), calculated as the difference in monthly mean T_s and LW between all-sky and cloud-free conditions, were highly correlated (R^2 = 0.68 for LWD and R^2 = 0.92 for LWU). Dramatic changes in T_s, CF and LW fluxes at Ny-Ålesund were closely associated with cold and warm air mass advection on a multi-day time scale. The average T_s under low-level clouds (LCBH ≤ 2 km) was estimated as −7.4 ± 6.1 °C due to warm air masses advected from the North Atlantic Ocean and Barents Sea, whereas the average T_s on cloud-free days was −14.5 ± 5.7 °C because of cold air mass advection from the pole. However, the duration of low-level clouds may not be long enough to drive such large T_s variations. 75-percentile of low-level cloud conditions at Ny-Ålesund persisted up to 2.3 days, whereas cloud-free and high-altitude cloud (LCBH > 2 km) conditions lasted for approximately 0.8 and 0.5 days, respectively. This implies that cloud LW effects on several warm days may be larger than the monthly average, but may not be accumulated enough to induce surface warming due to abrupt T_s drop associated with cold air mass advection.

Keywords: Arctic clouds, longwave radiation, cloud fraction, cloud base height, Ny-Ålesund

1. Introduction

Arctic clouds play a key role in the surface radiation budget by modulating longwave (LW) and shortwave (SW) radiative fluxes, which affect surface temperature and the extent of sea ice and snow melting (Curry et al., 1996). Clouds in the Arctic are also well known as one of major contributors to Arctic amplification (Graversen and Wang 2009; Cronin and Tziperman, 2015). Clouds mainly have a warming effect but sometimes a cooling effect lies in the surface albedo. Several intensive experiments, such as the Surface Heat Budget of the Arctic Ocean (SHEBA; Uttal et al., 2002) and Arctic Summer Cloud Ocean Study (ASCOS; Tjernström et al., 2014), have revealed that clouds warm the Arctic surface for most of the annual cycle, but cool the surface in mid-summer (Intrieri et al., 2002; Shupe and Intrieri, 2004) when a melting of sea ice has already started due to increased downward SW so that the surface albedo is lowered. Decreased cloud cover in the summer can directly reduce sea ice extent due to increased solar radiation reaching the surface (Kay et al., 2008; Kay and Gettelman, 2009), whereas decreased wintertime cloud cover, which potentially decreases the surface warming, may have an important role in sea ice cover return the following summer (Liu and Key, 2014).

Investigating cloud-radiative interactions in the Arctic is still challenging due to complex environmental conditions (e.g. low temperature and absolute humidity, persistent temperature inversions, highly reflective and inhomogeneous snow/ice surface and multi-layered clouds; Curry et al., 1996; Stamnes

*Corresponding author. e-mail: sangwookim@snu.ac.kr

Citation: Tellus B: 2018, **70**, 1450589, http://dx.doi.org/10.1080/16000889.2018.1450589

et al., 1999) and cloud microphysics (e.g. liquid or solid particles and cloud base temperature; Earle et al., 2011). Cloud radiative effects are also largely affected by the surface albedo and solar zenith angle (Shupe and Intrieri, 2004; Sedlar et al., 2011).

In addition, Arctic surface radiative fluxes among atmosphere-only models show large uncertainties, especially for cloudy conditions (Walsh et al., 2002). Cloud simulations and intercomparisons from Arctic regional climate models have shown considerable differences in cloud fraction (CF) and cloud microphysics (e.g. liquid water path) compared to observational data (Tjernström et al., 2008; Wyser et al., 2008). Moreover, reanalysis data show large discrepancies compared to ground-based and satellite observations of the radiation budget and CF over the Arctic (Zygmuntowska et al., 2012; Chaudhuri et al., 2014). These deficiencies still provide large uncertainties in estimating Arctic cloud radiative effects.

In this study, we investigated monthly variations in cloudiness and their impacts on the surface LW radiation budget and near-surface temperature (T_s) using a 10-year (2004–2013) observation record of cloud geometry properties, surface SW and LW radiation, and meteorological parameters at Ny-Ålesund, Svalbard. We also investigated the influence of warm and cold air mass advection related to regional-scale atmospheric circulations on cloudiness, surface LW fluxes and T_s during winter.

2. Cloud and surface radiation data

Comprehensive surface observations of cloud and surface radiation budget were made from January 2004 to December 2013 at Ny-Ålesund (78.92°N, 11.53°E), on the island of Spitsbergen in Svalbard, Norway.

Lowest cloud base height (LCBH) and CF were estimated from cloud vertical structure measurements using a Micro-Pulse Lidar (MPL; Spinhirne, 1993; Shiobara et al., 2003), operated by National Institute of Polar Research (NIPR) as part of NASA's Micro-Pulse Lidar Network (MPLNET). The Normalized Relative Backscatter (NRB) profile, averaged over 1-min time intervals and 30-m vertical resolution, at a wavelength of 523 nm was used to estimate the LCBH. To match with radiation data, LCBH was calculated as the mean value of CBH when clouds were observed for more than 25 min in MPL observations for 30 min. It is worth to mention that LCBH was only used in this study because we cannot get accurate information on cloud top height for optically thick clouds and on cloud boundaries for multi-layered clouds due to strong signal attenuation inside clouds. Following the method provided in Dong et al. (2010), we calculated CF as the percentage of lidar returned signals that were detected as clouds (i.e. the ratio of cloud detection number to total observation number) within a specific sample period (e.g. day or month). Here, we note that lidar-derived CF, which accounts for the presence of clouds along the laser beam path, may be different compared to routine observations estimating the fraction of sky covered by cloud at a given time, depending on how clouds were distributed. Compared to the regular routine observation of hemispheric cloud coverage, near-zenith viewing lidar-derived CF can be overestimated when most clouds were present along the lidar beam path but no clouds in the sky around, and *vice versa*.

The Korea Polar Research Institute (KOPRI) measured the hemispheric downwelling and upwelling shortwave (SWD and SWU; 0.3–2.8 μm) and longwave (LWD and LWU; approximately 5–50 μm) irradiances with Kipp & Zonen pyranometers and pyrgeometers (model: CNR1). The radiation measurements were located about 300 m away from the ocean water and about 1.3 km from the Zeppelin Mountain (472 m, above mean sea level). The upwelling and downwelling data presented in this paper were collected at the same location as the MPL measurements. Surface SW and LW fluxes used in this study were in agreement with co-located (about 100 m away) and simultaneous flux measurements within the framework of Baseline Surface Radiation Network (BSRN). The absolute value of mean difference between the two was about 1.3 W m^{-2} (SWD), 0.7 W m^{-2} (SWU), 1.0 W m^{-2} (LWD) and 1.1 W m^{-2} (LWU), and the root mean square was about 10.5 W m^{-2} (SWD), 8.3 W m^{-2} (SWU), 4.4 W m^{-2} (LWD) and 4.1 W m^{-2} (LWU), respectively. In addition, meteorological measurements, including temperature, relative humidity, wind speed and direction at the ground level were made by KOPRI.

3. Monthly variations of cloud fraction and surface radiation

Figure 1a shows the monthly variation in CF along with the six LCBH categories derived from MPL measurements from 2004 to 2013. The mean annual CF was 0.84 ± 0.05, and increased from February (0.74) to May (0.88), remained relatively high from May to September (~0.91), and then decreased from October to February. CFs at Ny-Ålesund from May to October are similar to those reported from radar–lidar measurements at Barrow, Alaska, but CFs from January to April are slightly higher than those observed at Barrow (Dong et al., 2010). This difference is due to the location of Ny-Ålesund at the northernmost point of North Atlantic cyclone track, therefore the site is frequently influenced by cyclone from the Atlantic (Kim et al., 2017).

The minimum CF for LCBH below 1 km (LCBH ≤ 1 km) appeared in March (0.16), whereas the maximum was in July (0.49). The percentage of CF for LCBH ≤ 1 km increased in summer warm months due to the formation of optically thick near-surface clouds from enhanced sea to atmosphere heat and moisture flux (e.g. Ganeshan and Wu, 2016). Lower (sub-freezing) temperatures would increase the likelihood of ice clouds (or ice concentration in clouds) that more readily falls out and

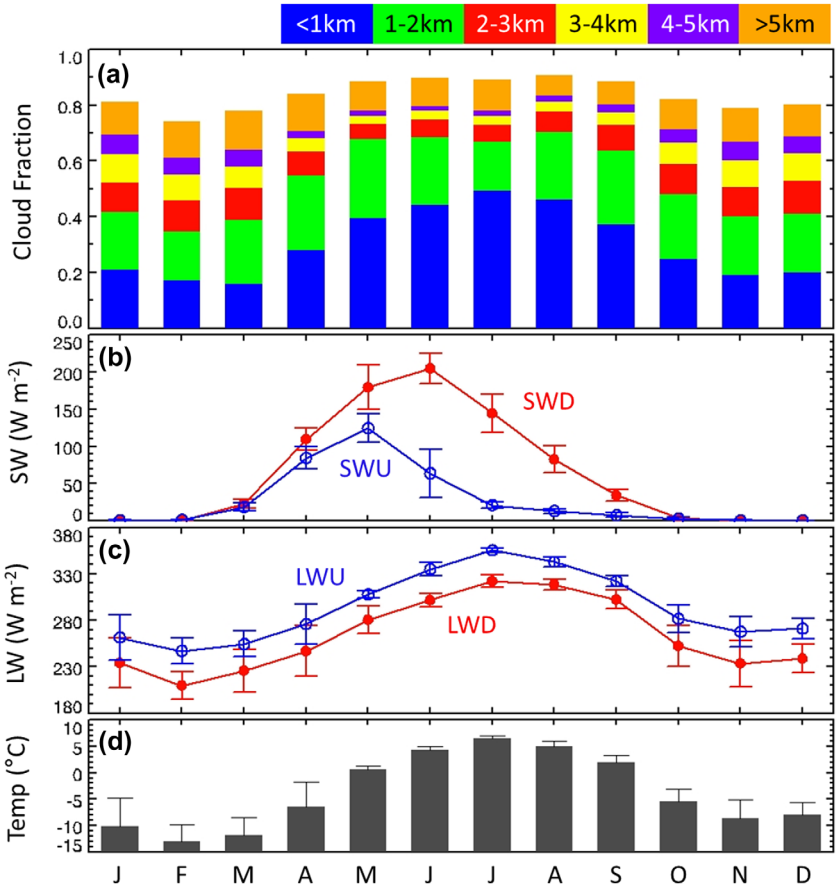

Fig. 1. Variations in monthly averages of (a) cloud fractions with the six-categorized lowest cloud base heights; upward and downward (b) shortwave and (c) longwave fluxes; and (d) near-surface air temperature at Ny-Ålesund, Svalbard from 2004 to 2013.

therefore reduces the cloud fraction during winter. Frequent horizontal transport of dry cold air masses over ice sheet from central Arctic also can be attributed to lower percentage of CF for LCBH ≤ 1 km during winter. In contrast with the CF for LCBH ≤ 1 km, the CF for LCBH > 2 km was the lowest in summer (i.e. January: 0.40, August: 0.20). As we mentioned above, the ground-based up-looking lidar cannot properly measure clouds overlying optically thick clouds due to signal attenuation.

Figure 1b illustrates the monthly mean and standard deviation of the SW flux. The downward SW (SWD) flux peaked in June (205 W m^{-2}), when sunshine duration and solar elevation were the highest, while the SWD flux was zero during the polar night, from November to February. The upward SW (SWU) flux, which is equal to the reflected SWD flux, depends on surface albedo and SWD flux.

The SWU flux increased from zero in winter to 18 W m^{-2} in March, 124 W m^{-2} in May, and then sharply decreased from June (64 W m^{-2}). Unlike SWD, maximum SWU occurred in May, because of the reduction in surface albedo due to the snow melt (Dong et al., 2010; Maturilli et al., 2015). The inter-annual standard deviation in SWU flux was the highest in June (32 W m^{-2}), because the initiation of surface snow/ice melting was slightly different each year (Maturilli et al., 2015).

Figure 1c shows the monthly mean and standard deviation of the LW fluxes from ground-based radiation measurements. Because the upward LW (LWU) flux is primarily dependent on the surface temperature and emissivity, the LWU flux showed a maximum of 355 W m^{-2} in July and a minimum of 247 W m^{-2} in February, which is similar to the annual variation in near-surface temperature (T_s; maximum in July: 6.5 °C, minimum in February: –13.1 °C; see Fig. 1d). The magnitude of LWD flux is affected by atmospheric moisture and cloud properties, such as cloud optical thickness and cloud base temperature. Compared to summer (e.g. 322 W m^{-2} for July), the LWD flux observed in winter was much lower (e.g. 210 W m^{-2} for February) at Ny-Ålesund because the amount of atmospheric water vapour, air temperature and CF were low in winter (Maturilli and Kayser, 2017).

Meanwhile, the large atmospheric moisture in summer can make LWD flux less sensitive to presence of low-level clouds, which caused lower inter-annual variation of LWD flux in

summer (standard deviation in JJA: 6.5 W m^{-2}) than winter (standard deviation in DJF: 19.0 W m^{-2}). This result is consistent with those observed at Barrow, Alaska (Dong et al., 2010).

4. Relation between cloud parameters and longwave radiation in winter: a monthly perspective

In this section, we provide a discussion on the relationship between cloud geometry properties (i.e. LCBH, CF) and surface LW fluxes, as well as between cloud LW radiative effects and T_s. To exclude the effect of SW flux on T_s, the analysis focused only on wintertime, November to February.

Figure 2 shows the surface LWD and LWU fluxes during the winter periods from 2004 to 2013 with respect to LCBH every kilometre. It should be noted that the LWD flux at the surface depends on cloud height and amount as well as atmospheric temperature and humidity, whereas the LWU is entirely dependent on T_s, which is affected by LWD as well as many other factors (e.g. SWD, warm advection). Both LWD and LWU fluxes in the cloud-free condition were lower than those in cloudy condition. The surface LWD flux increased as LCBH decreased, due to increasing cloud radiating temperature with lower LCBH, relating also with atmospheric temperature. The LWD flux increased by approximately 83 W m^{-2} from the cloud-free (182 ± 26 W m^{-2}) to cloudy condition for LCBH ≤ 1 km (265 ± 35 W m^{-2}), and gradually decreased with increasing LCBH (e.g. 208 ± 35 W m^{-2} for LCBH ≥ 4 km). The surface LWU flux showed similar variation, but having a small magnitude variation with increasing LCBH. The LWU flux difference between the cloud-free condition and LCBH ≤ 1 km (LCBH > 4 km, in parenthesis) was estimated to be approximately 40 W m^{-2} (16 W m^{-2}). The net LW (LWN), calculated by subtracting the LWU flux from the LWD flux, increased from –55 W m^{-2} for the clear-sky condition to –12 W m^{-2} for LCBH ≤ 1 km. This result suggests that low-level clouds reduced radiative cooling (i.e. increasing surface radiative warming) during winter at Ny-Ålesund, as indicated by positive cloud radiative forcing (CRF).

Figure 3 is a scatter plot of monthly averaged CF derived from MPL measurements and surface LW fluxes at Ny-Ålesund during the winter periods from 2004 to 2013. Both monthly averaged LWU and LWD fluxes increased as monthly averaged CF increased. Because the slope was about 110 (i.e. 110 W m^{-2} per unit CF) for the LWU flux and 160 (i.e. 160 W m^{-2} per unit CF) for the LWD flux, the difference between the LWD and LWU fluxes monotonically reduced with increasing CF. From Figs. 2 and 3, we can conclude that the LWN increases with decreasing LCBH and increasing CF. Shupe and Intrieri (2004) also found that CRF increased with decreasing LCBH and increasing CF, based on LW flux measurements at SHEBA and clear-sky radiation derived from the radiative transfer model.

Figure 4 shows the relationship between near-surface temperature difference (ΔT_s) and downward (ΔLWD) and upward LW (ΔLWU) radiation difference for a month and 30-min averaged data. Here, ΔLWD, ΔLWU and ΔT_s were calculated as the differences in LWD, LWU and T_s between 30-min data and monthly mean data under cloud-free conditions for that month (Ramanathan et al., 1989). Monthly averaged ΔLWD showed a positive correlation with ΔT_s (R^2 = 0.68; Fig. 4a). Meanwhile, the 30-min averaged ΔT_s and ΔLWD data were more widely scattered even though the coefficient of determination was similar (R^2 = 0.66). The 30-min averaged data were clearly divided into two groups: one was distributed in the range of ±5 °C and ±20 W m^{-2} centred both ΔT_s and ΔLWD on zero (hereafter, 'cold group'; black dotted box), and the other group was distributed over 5–15 °C and 40 – 120 W m^{-2} (hereafter, 'warm group'; red dotted box).

As with the monthly average data, ΔLWD in warm group increased with ΔT_s and the slope of ΔLWD was similar to that of monthly average data. This high ΔLWD and its good relation to ΔT_s can be attributable to the presence of low-level clouds,

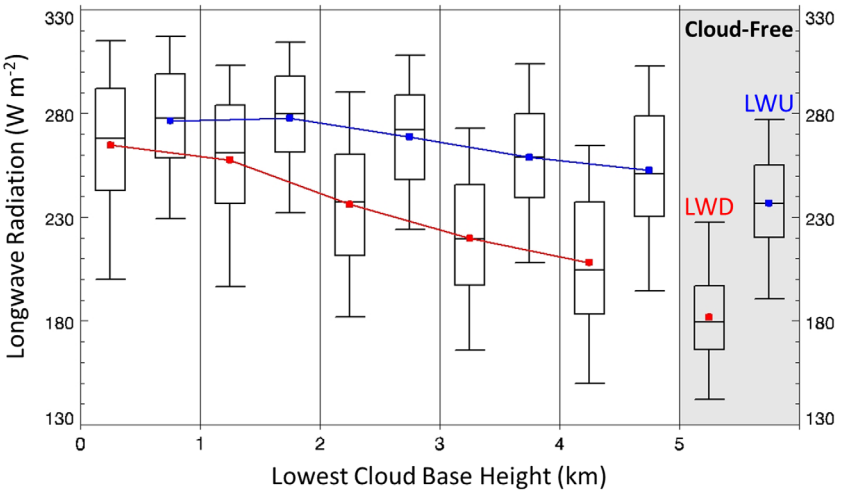

Fig. 2. Relationship between longwave radiation and lowest cloud base height during winter, November–February. The longwave fluxes for wintertime cloud-free conditions are also provided. In the box-whisker plot, the 25th and 75th percentiles bound the centre box with the horizontal line representing the 50th percentile, or median, and the dot depicts the mean.

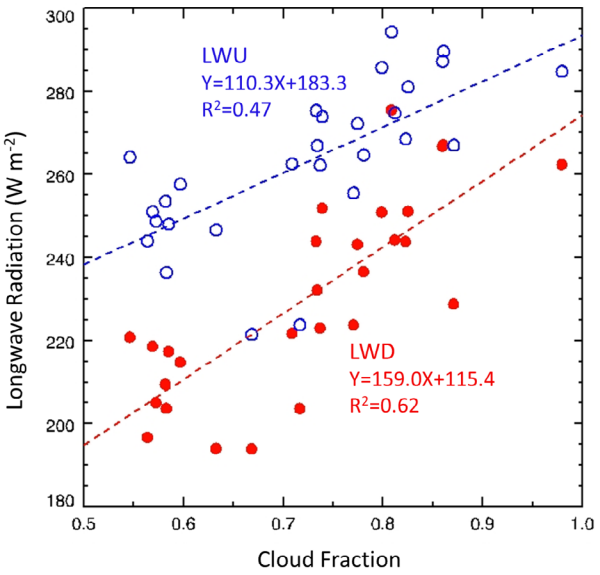

Fig. 3. Scatter plot of monthly mean upward (blue empty circle) and downward (red full circle) longwave fluxes and cloud fraction during the winter periods, November–February, of 2004–2013.

as expected from Fig. 2. Larger change (i.e. lower slope) in ΔT_s relative to ΔLWD in cold group was observed under cloud-free condition or mid- and high-level clouds (more detailed discussion in Section 5). As shown in Fig. 4b, ΔLWU also linearly increased as ΔT_s increased both in 30 min ($R^2 = 0.93$) and monthly ($R^2 = 0.92$) averaged data, because the LWU flux is primarily dependent on the surface temperature. An increase in ΔLWD can result in an increase of T_s, which subsequently contributes to an increase of LWU. The monthly mean ΔLWD and ΔLWU of this study were similar to those reported in previous studies (Shupe and Intrieri, 2004; Dong et al. 2010). However, the CRF may not be the only driver changing the ΔT_s from –10 to 15 °C, as shown in the 30-min average data. Compared to monthly average data, a large variation in the 30-min averaged ΔLWD (–40 – 140 W m^{-2}) and ΔLWU (–40 – 100 W m^{-2}) was also observed. To further explain the possible factors influencing T_s, we investigated changes in CF, LCBH, LW fluxes and T_s under varying regional-scale circulations (i.e. advection of cold or warm air mass) on a multi-day time scale over the study region.

5. Effects of air mass advection on surface LW fluxes and temperature on a multi-day time scale

Distinct changes in cloudiness, T_s and fluxes on a multi-day time scale associated with regional-scale circulation were very often observed at Ny-Ålesund during the winter. As an example, Figure 5 shows the temporal variations in LCBH, surface LW fluxes, and T_s at Ny-Ålesund from 1 to 10 February 2010. Both surface LWD flux and T_s dramatically changed every two days in this case. On cold days (T_s: −8 to −10 °C), LWD flux was about 220 to 230 W m^{-2} under cloud-free conditions (e.g. 6–7 February) and high clouds (LCBH ≥ 6 km; 3 February), whereas an LWD flux of ~300 W m^{-2} was observed on warm days (−2 to −1 °C, 4–5 and 8–9 February) under low-level clouds (LCBH ≤ about 2 km). In addition, the LWD flux and T_s sharply increased about 60 W m^{-2} and 4 °C, respectively, within a few hours around 00 UTC on 4 February 2010. Similar drastic decreases were observed on 6 February 2010. The temporal variation in the LWU flux was similar to the LWD flux, but with a small fluctuation. T_s was a relatively constant and LWN was near zero on warm days under low-level clouds, while T_s dropped and LWN was estimated at about −40 to −50 W m^{-2} during cloud-free condition. The variation of LWN is consistent with observations under clear and cloudy conditions at the SHEBA site during winter (Stramler et al., 2011).

However, under switching of warm and cold air masses with about a two-day cycle, low-level clouds are not solely responsible for abrupt changes of surface LW fluxes and T_s on warm days. This is because increases in LWD flux and T_s were simultaneously observed when warm air mass advected over the site. To further explain the relationships between clouds, LWD flux and T_s at Ny-Ålesund, we investigate the T_s distribution frequency with respect to cloud-free and cloudy (LCBH ≤ 2 km and LCBH > 2 km) conditions during the winter periods from 2004 to 2013 (Fig. 6). Mean T_s for cloud-free conditions was estimated as –14.5±5.7 °C, but mean T_s under low-level clouds was –7.4 ± 6.1 °C. As we explained in Fig. 5, changes in T_s were closely associated with the presence of low-level clouds. However, the duration of low-level cloud (approximately 2 days in Fig. 5) may not be long enough to drive such large T_s changes. 75-percentile (95-percentile, in parenthesis) of low-level cloud conditions (LCBH ≤ 2 km) at Ny-Ålesund were estimated to persist up to approximately 2.3 (5.8) days from MPL measurements (Fig. 7). Cloud-free and high-altitude cloud (LCBH > 2 km) conditions lasted for approximately 0.8 (2.1) and 0.5 (1.4) days at the 75-percentile (95-percentile), respectively.

To investigate the relationship between regional-scale circulations and the observed clouds in Ny-Ålesund, we plot the averaged geopotential height and wind fields at 850 hPa pressure level during winter in 2004–2013 (Fig. 8). Generally, the semi-permanent Icelandic low is located at the south of Greenland (denoted as 'L' in Fig. 8a), which can affect the cyclone activity such as track and intensity over Arctic during winter (Serreze et al., 1997; Fig. 8a). According to Brümmer et al. (2000), an active cyclogenesis is frequently observed over the Fram Strait between Greenland and Spitsbergen. When low-level clouds (LCBH ≤ 2 km) were observed at Ny-Ålesund (Fig. 8b), warm and moist air were brought from North Atlantic Ocean into the Spitsbergen by southerly/south-westerly winds, which were enhanced by deepening Icelandic low-pressure system. This is also clearly seen in the backward trajectory

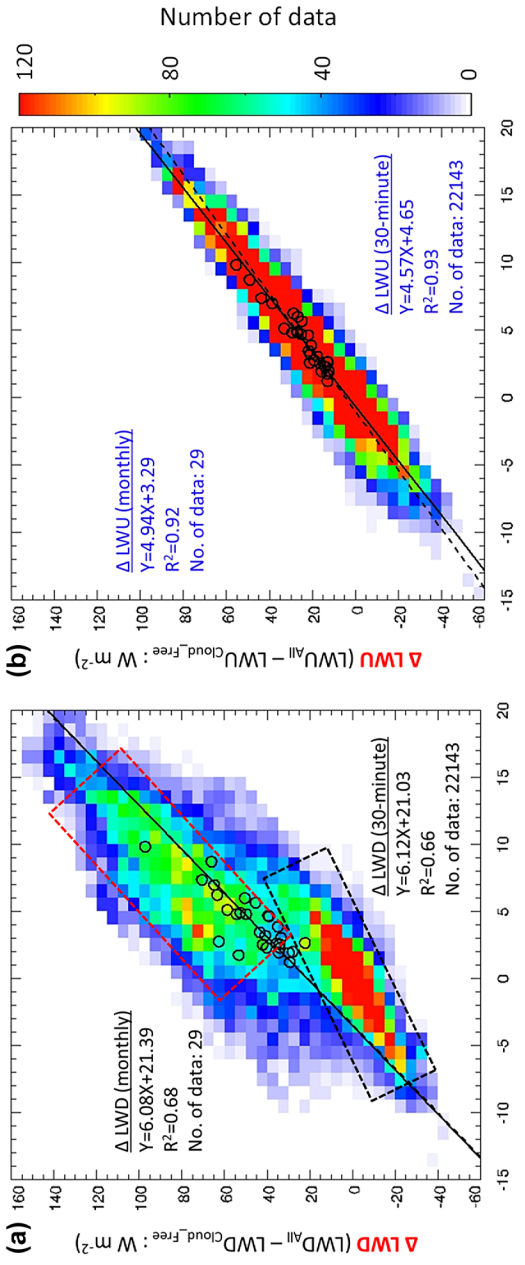

Fig. 4. Relationship between near-surface temperature difference and downward (left panel) and upward (right panel) longwave radiation difference for monthly (black open circle) and 30-min (data points expressed in colour) averaged data during the winter periods, November–February, of 2004–2013. Temperature and downward and upward longwave differences are calculated between all-sky and cloud-free conditions. The solid and dashed lines represent the least-square linear regression for monthly and 30-min averaged data, respectively.

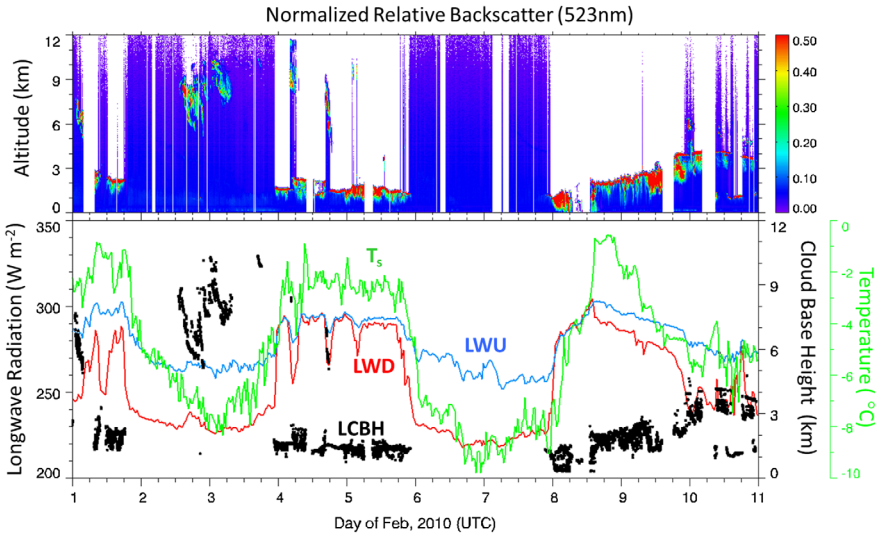

Fig. 5. Cloud, longwave radiation and near-surface temperature measurements at Ny-Ålesund, Svalbard, from 1 to 10 February 2010: (upper panel) Lidar-derived backscattering intensity at 523-nm wavelength, (lower panel) near-surface temperature (T_s; green), upward (blue) and downward (red) longwave radiation (LWU, LWD) and cloud base height (LCBH; black dot) estimated from lidar measurements.

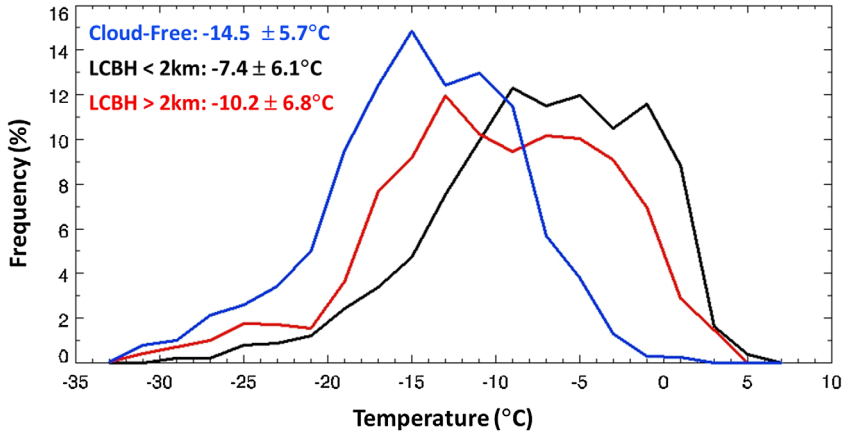

Fig. 6. Frequency distribution (%) of near-surface temperature for cloud-free (blue), LCBH < 2 km (black) and LCBH > 2 km (red) conditions.

analysis (Fig. S1). On the other hand, cold and dry air masses were advected from central Arctic and north of Barents Sea into Ny-Ålesund by north-easterly winds on cloud-free days at Ny-Ålesund (Figs. 8c and S1). This is associated with strongly developed high pressure over Greenland and low pressure over Norwegian Sea and Barents Sea, and a weakening of the Icelandic Low.

The ΔT_s was positively correlated with CRF (ΔLWD) when calculated from monthly mean data as shown in Fig. 4. It should be noted that the CRF on several warm days may be larger than the monthly average, but may not be accumulated enough to induce surface warming due to abrupt T_s drop associated with cold air mass advection. To more accurately estimate the effects of clouds on LW fluxes and T_s, regional-scale circulations should be also considered over areas with observed short-period warm and cold air mass advection, such as Ny-Ålesund.

6. Summary

We analyse monthly variations in clouds and surface SW and LW fluxes using a 10-year period (2004–2013) of observations at Ny-Ålesund, Svalbard. We also investigated the relationship between clouds and surface LW fluxes, and the influence of warm and cold air mass advection due to regional-scale atmospheric circulation on winter cloudiness, surface LW fluxes and T_s. The principal findings of our analysis are summarized below:

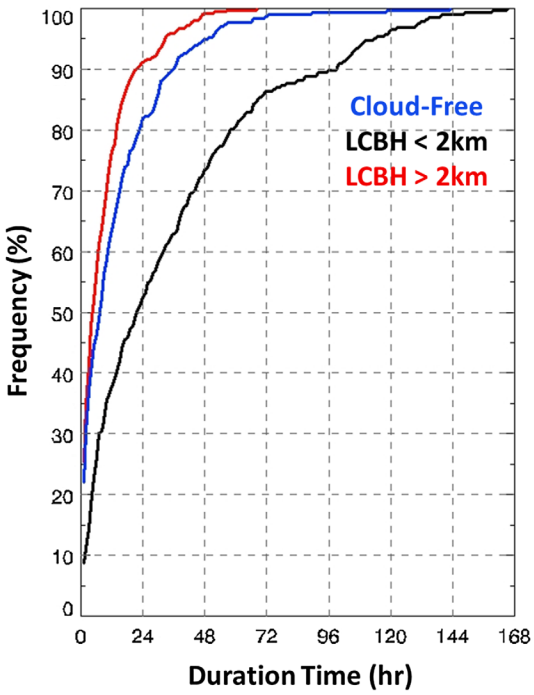

Fig. 7. Cumulative frequency distribution (%) of cloud duration (in hours) for cloud-free (blue), LCBH < 2 km (black) and LCBH > 2 km (red).

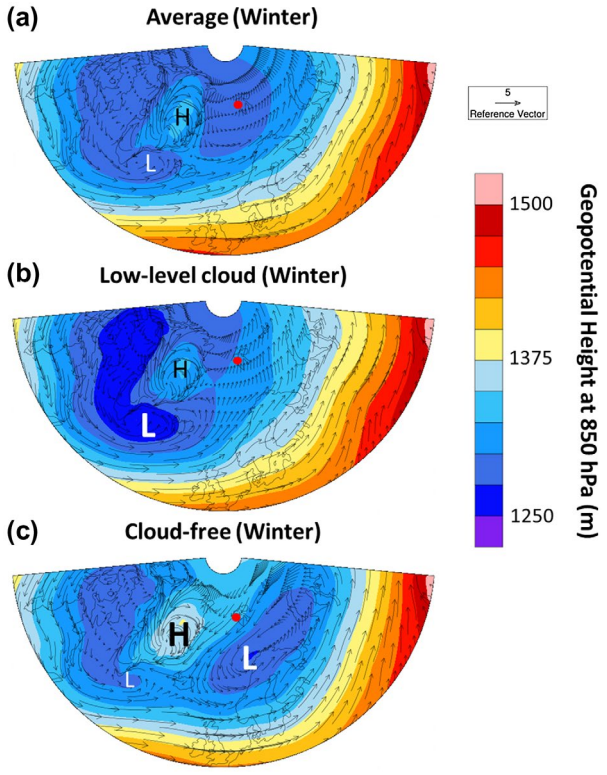

Fig. 8. Geopotential height and wind field at 850 hPa pressure level over North Atlantic sector of Arctic during winter averaged from 2004 to 2013: (a) overall period, (b) low-level cloud conditions and (c) clear conditions at Ny-Ålesund. The red dot indicates the location of Ny-lesund station.

- The CF derived from MPL showed distinct monthly variations, having higher CF in summer (July: 0.9) and lower CF in winter (February: 0.79). The SWD flux increased monotonically from March and showed a peak (~200 W m^{-2}) in June. In contrast, the LWD flux gradually increased from ~200 W m^{-2} in February to ~300 W m^{-2} in July.
- Both LWD and upward LW (LWU) fluxes and their difference (LWN) increased during winter as the lowest cloud base height (LCBH) decreased and CF increased.
- Monthly averaged ΔLWD showed a positive correlation with ΔT_s (R^2 = 0.68), whereas the 30-min averaged ΔT_s and ΔLWD data were more widely scattered even though the coefficient of determination was similar (R^2 = 0.66). ΔLWU linearly increased as ΔT_s increased both in 30 min (R^2 = 0.93) and monthly (R^2 = 0.92) averaged data, which implies that an increase in LWN flux may influence the T_s increase. Although the monthly mean ΔLWD and ΔLWU of this study were similar to those reported in previous studies, the CRF may not be the only driver changing the ΔT_s from –10 to 15 °C, as shown in the 30-min average data.
- Dramatic changes in the T_s, CF and LWD flux at Ny-Ålesund on a multi-day time scale were closely linked with cold and warm air mass advection.
- The mean T_s under low-level clouds (LCBH ≤ about 2 km) was estimated as –7.4 ± 6.1 °C due to relatively warm air masses advected from the North Atlantic Ocean and Barents Sea. In contrast, the mean T_s on cloud-free days was –14.5 ± 5.7 °C because of cold air mass advection from the pole. However, the duration of low-level clouds may not be enough to drive T_s variations due to switching of cold and warm advection over Ny-Ålesund. 75-percentile (95-percentile) of low-level cloud conditions (LCBH ≤ 2 km) at Ny-Ålesund persisted up to approximately 2.3 (5.8) days, whereas cloud-free and high-altitude cloud (LCBH > 2 km) conditions lasted for 0.8 (2.1) and 0.5 (1.4) days at the 75-percentile (95-percentile), respectively. This implies that shorter episodes may have a much larger CRF than the monthly average, but the CRF during warm air mass advection period may not be accumulated enough to induce surface warming due to abrupt T_s drop by cold air mass advection. More explicitly, changes in surface LW fluxes and T_s associated with regional-scale circulations may not be reflected in monthly or seasonally averaged data. Therefore, high-temporal resolution cloud and LW flux data should be used to more accurately estimate cloud LW effects in the North Atlantic sector of the Arctic during winter.

Better coordinated observation and modelling studies will be needed to advance our understanding of the effects of cloud LW radiative forcing and air mass advections on surface temperature. Especially, intensive ground-based and airborne observations for vertical profiles of cloud microphysical properties (e.g.

phase and effective radius of cloud particles, ice/liquid water content), meteorological parameters and LW/SW net radiation fluxes over Ny-Ålesund and surrounding regions will help to explain the effect of synoptic circulation on cloudiness at Ny-Ålesund and to more precisely estimate the LW effects of clouds.

Acknowledgements

The authors are very grateful to two anonymous reviewers for their thoughtful comments and insightful suggestions.

Disclosure statement

No potential conflict of interest was reported by the authors.

Funding

This study was supported by Korea Polar Research Institute [PE18130].

Supplemental data

Supplemental data for this article can be accessed here https://doi.org/10.1080/16000889.2018.1450589.

References

Brümmer, B., Thiemann, S. and Kirchgäßner, A. 2000. A cyclone statistics for the Arctic based on European Centre re-analysis data. *Meteorol. Atmos. Phys.* **75**, 233–250.

Chaudhuri, A. H., Ponte, R. M. and Nguyen, A. T. 2014. A comparison of atmospheric reanalysis products for the Arctic ocean and implications for uncertainties in air–sea fluxes. *J. Clim.* **27**, 5411–5421.

Cronin, T. W. and Tziperman, E. 2015. Low clouds suppress Arctic air formation and amplify high-latitude continental winter warming. *Proc. Nat. Acad. Sci.* **112**, 11490–11495.

Curry, J. A., Schramm, J. L., Rossow, W. B. and Randall, D. 1996. Overview of Arctic cloud and radiation characteristics. *J. Clim.* **9**, 1731–1764.

Dong, X., Xi, B., Crosby, K., Long, C. N., Stone, R. S. and co-authors. 2010. A 10 year climatology of Arctic cloud fraction and radiative forcing at Barrow, Alaska. *J. Geophys. Res. Atmos.* **115**, D17212 (1–14 pages). doi:10.1029/2009JD013489.

Earle, M. E., Liu, P. S. K., Strapp, J. W., Zelenyuk, A., Imre, D. and co-authors. 2011. Factors influencing the microphysics and radiative properties of liquid-dominated Arctic clouds: Insight from observations of aerosol and clouds during ISDAC. *J. Geophys. Res.* **116**, D00T09 (1–16 pages). doi:10.1029/2011JD015887.

Ganeshan, M. and Wu, D. L. 2016. The open-ocean sensible heat flux and its significance for Arctic boundary layer mixing during early fall. *Atmos. Chem. Phys.* **16**, 13173–13184.

Graversen, R. G. and Wang, M. 2009. Polar amplification in a coupled climate model with locked albedo. *Clim. Dyn.* **33**, 629–643.

Intrieri, J., Fairall, C., Shupe, M., Persson, P., Andreas, E. and co-authors. 2002. An annual cycle of Arctic surface cloud forcing at SHEBA. *J. Geophys. Res. Oceans* **107**, 8030 (1–15). doi:10.1029/2000JC000423.

Kay, J. E. and Gettelman, A. 2009. Cloud influence on and response to seasonal Arctic sea ice loss. *J. Geophys. Res. Atmos.* **114**, D18204 (1–18 pages), doi:10.1029/2009JD011773.

Kay, J. E., L'Ecuyer, T., Gettelman, A., Stephens, G. and O'Dell, C. 2008. The contribution of cloud and radiation anomalies to the 2007 Arctic sea ice extent minimum. *Geophys. Res. Lett.* **35**, L08503 (1–5 pages). doi:10.1029/2008GL033451.

Kim, B.-M., Hong, J.-Y., Jun, S.-Y., Zhang, X., Kwon, H. and co-authors. 2017. Major cause of unprecedented Arctic warming in January 2016: Critical role of an Atlantic windstorm. *Scientific Reports* **7**, 40051 (1–9 pages). doi:10.1038/srep40051.

Liu, Y. and Key, J. R. 2014. Less winter cloud aids summer 2013 Arctic sea ice return from 2012 minimum. *Environ. Res. Lett.* **9**, 044002.

Maturilli, M., Herber, A. and König-Langlo, G. 2015. Surface radiation climatology for Ny-Ålesund, Svalbard (78.9° N), basic observations for trend detection . *Theor. Appl. Climatol.* **120**, 331–339.

Maturilli, M. and Kayser, M. 2017. Arctic warming, moisture increase and circulation changes observed in the Ny-Ålesund homogenized radiosonde record. *Theor. Appl. Climatol.* **130**, 1–17.

Ramanathan, V., Cess, R., Harrison, E., Minnis, P. and Barkstrom, B. 1989. Cloud-radiative forcing and climate: Results from the earth radiation budget experiment. *Science* **243**, 57–63.

Sedlar, J., Tjernström, M., Mauritsen, T., Shupe, M. D., Brooks, I. M. and co-authors. 2011. A transitioning Arctic surface energy budget: The impacts of solar zenith angle, surface albedo and cloud radiative forcing. *Clim. Dyn.* **37**, 1643–1660.

Serreze, M. C., Carse, F., Barry, R. G. and Rogers, J. C. 1997. Icelandic low cyclone activity: Climatological features, linkages with the NAO, and relationships with recent changes in the northern hemisphere circulation. *J. Clim.* **10**, 453–464.

Shiobara, M., Yabuki, M. and Kobayashi, H. 2003. A polar cloud analysis based on Micro-pulse Lidar measurements at Ny-Alesund, Svalbard and Syowa, Antarctica. *Phys. Chem. Earth, Parts A/B/C* **28**, 1205–1212.

Shupe, M. D. and Intrieri, J. M. 2004. Cloud radiative forcing of the Arctic surface: The influence of cloud properties, surface albedo, and solar zenith angle. *J. Clim.* **17**, 616–628.

Spinhirne, J. D. 1993. Micro pulse lidar. *IEEE Trans. Geosci. Remote Sens.* **31**, 48–55.

Stamnes, K., Ellingson, R. G., Curry, J. A., Walsh, J. E. and Zak, B. D. 1999. Review of science issues, deployment strategy, and status for the ARM North Slope of Alaska–adjacent Arctic Ocean climate research site. *J. Clim.* **12**, 46–63.

Stramler, K., Del Genio, A. D. and Rossow, W. B. 2011. Synoptically driven Arctic winter states. *J. Clim.* **24**, 1747–1762.

Tjernström, M., Leck, C., Birch, C. E., Bottenheim, J. W., Brooks, B. J. and co-authors. 2014. The Arctic Summer Cloud Ocean Study (ASCOS): Overview and experimental design. *Atmos. Chem. Phys.* **14**, 2823–2869.

Tjernström, M., Sedlar, J. and Shupe, M. D. 2008. How well do regional climate models reproduce radiation and clouds in the Arctic? An evaluation of ARCMIP simulations. *J. Appl. Meteorol. Climatol.* **47**, 2405–2422.

Uttal, T., Curry, J. A., Mcphee, M. G., Perovich, D. K., Moritz, R. E. and co-authors. 2002. Surface heat budget of the Arctic ocean. *Bull. Am. Meteorol. Soc.* **83**, 255–275.

Walsh, J. E., Kattsov, V. M., Chapman, W. L., Govorkova, V. and Pavlova, T. 2002. Comparison of Arctic climate simulations by uncoupled and coupled global models. *J. Clim.* **15**, 1429–1446.

Wyser, K., Jones, C. G., Du, P., Girard, E., Willén, U. and co-authors 2008. An evaluation of Arctic cloud and radiation processes during the SHEBA year: Simulation results from eight Arctic regional climate models. *Clim. Dyn.* **30**, 203–223.

Zygmuntowska, M., Mauritsen, T., Quaas, J. and Kaleschke, L. 2012. Arctic clouds and surface radiation – A critical comparison of satellite retrievals and the ERA-interim reanalysis. *Atmos. Chem. Phys.* **12**, 6667–6677.